Mass Transfer of a Thermally Radiative MHD Cattaneo-Christov Nanofluid between Two Stretchable Spinning Disks

(Pemindahan Jisim Radiatif Terma Bendalir MHD Cattaneo-Christov antara Dua Cakera Berputar Meregang)

Peter Ngbo Habu[1,3], Sharifah Nuriza Al'Aidrus[1], Noor Fadiya Mohd Noor[1,2,*] & Zailan Siri[1,2]

[1]*Institute of Mathematical Sciences, Faculty of Science, Universiti Malaya, 50603 Kuala Lumpur, Federal Territory, Malaysia*

[2]*Center for Data Analytics Consultancy & Services, Faculty of Science, Universiti Malaya, 50603 Kuala Lumpur, Federal Territory, Malaysia*

[3]*Department of Mathematics, Faculty of Science, Federal University of Lafia, 950101 Nasarawa State, Nigeria*

ABSTRACT

The investigation on the impacts of magnetic field, thermal radiation, generation of heat and mass transfer in a porous-medium-embedded homogenous nanofluid flow between two stretchable spinning disks is crucial since spinning disks are prevalent in many engineering and technological applications. The objective of this research was to analyze the influences of these parameters using the Cattaneo-Christov heat flux model against the flow's temperature, velocity and concentration profiles. Temperature profile is a decreasing function of thermal relaxation time parameter due to the particles require a longer period to transfer heat to the next particles. The rates of heat transfer at both spinning disks decrease as values of heat generation, Eckert number, Prandtl number, Brownian diffusion, thermophoresis diffusion and rotation ratio increase. The disks' rates of mass transfer decrease with more thermophoresis diffusion, heat generation, heat transfer dissipation, and momentum diffusivity, but they increase with thermal radiation parameter. The current work attempts to include the transport profile of a Buongiorno's nanofluid embedded in a Darcian porous medium between dual spinning disks with magnetic field, thermal radiation and generation of heat using the heat flux model of Cattaneo-Christov's. Von Karman transformations are utilized to transform the nonlinear partial differential equations of fluid dynamics into coupled nonlinear ordinary differential equations (ODEs). These coupled ODEs are later solved by employing a shooting method with MATLAB *bvp4c* algorithm. All numerical evidences from this investigation are conferred through tables and figures after validation of present computations.

Keywords: Heat generation; mass transfer; MHD Cattaneo-Christov nanofluid; thermal radiation; two stretchable spinning disks

ABSTRAK

Kajian kesan medan magnet, radiasi terma, penjanaan haba dan pemindahan jisim dalam medium berliang yang dialiri oleh bendalir nano homogen di antara dua cakera meregang yang berputar adalah penting kerana cakera berputar lazimnya terdapat dalam banyak aplikasi kejuruteraan dan teknologi. Objektif penyelidikan ini ialah untuk menganalisis pengaruh parameter menggunakan model fluks haba Cattaneo-Christov terhadap profil suhu, halaju dan kepekatan aliran. Profil suhu adalah fungsi yang menyusut dengan parameter masa keredaan terma kerana zarah memerlukan jangka masa yang lebih lama untuk memindahkan haba ke zarah seterusnya. Kadar pemindahan haba pada kedua cakera berputar menyusut apabila nilai penjanaan haba, nombor Eckert, nombor Prandtl, penyebaran Brownian, penyebaran termoforesis dan nisbah putaran meningkat. Kadar pemindahan jisim cakera berkurang dengan penyebaran termoforesis, penjanaan haba, pelesapan pemindahan haba dan penyebaran momentum, tetapi meningkat dengan parameter radiasi terma. Kajian ini cuba memasukkan profil pengangkutan bendalir nano Buongiorno melalui medium berliang Darcy di antara dua cakera berputar dengan medan magnet, radiasi terma dan penjanaan haba menggunakan model fluks haba Cattaneo-Christov. Transformasi Von Karman digunakan untuk mengubah persamaan pembezaan separa tak linear

bagi dinamik bendalir supaya menjadi persamaan pembezaan biasa (PPB) tak linear. Gandingan PPB ini kemudiannya diselesaikan dengan menggunakan kaedah pembedilan dengan algoritma MATLAB *bvp4c*. Semua bukti berangka daripada penyelidikan ini dinyatakan dalam jadual dan rajah setelah pengiraan semasa disahkan.

Kata kunci: Bendalir nano MHD Cattaneo-Christov; dua cakera meregang yang berputar; pemindahan jisim; penjanaan haba; radiasi terma

INTRODUCTION

According to Jyothi et al. (2018), flows by spinning disks are widely used in industrial and engineering processes, such as manufacturing and technology for food processing, coating for spinning, air machines for laundry, equipment for medicals, in laser scanning of microscope, injection and compression in molding machines, and blower impeller in centrifugal pumps. Nanofluid is a material that contains solid nanosized particles known as nanoparticles. Flows due to nanofluids are still being investigated by many researchers under different conditions. The objective of this study was to investigate the role of Cattaneo-Christov heat flux in a Darcy porous medium embedded with a nanofluid between two stretchable spinning disks and how it interacts with thermal radiation, heat generation, magnetic induction and Joule heating against the velocity, temperature and concentration profiles and against heat and mass transfer rates.

Khan et al. (2016) investigated the features of heat flux of Cattaneo-Christov and Fick's law in a laminar 3-D Burger's fluid flow across a stretching surface. The modifications of the heat flux theory by Fourier and the law of Fick's using heat energy and time relaxation in concentration have been done in their model. They also investigated the features of heterogeneous and homogeneous reactions. Similarity transformation was used to derive the ordinary differential equations (ODEs) that are not linear. Homotopy Analysis Method (HAM) was applied on the equations. The influence due to several coefficients of measuring hotness and coldness with the quantities of particles in a given space has been analyzed and discussed graphically. It is understood that the hotness/coldness and concentration fields decrease as the non-dimensional heat energy and relaxation time in concentration are enhanced. Equally they were of the view that the boundary layer thickness for the flow concentration adjusts with the increase of Deborah numbers whereas this same profile decreases as the ratio of Schmidt increases. They came with a conclusion that there is a potential for the thermal distribution to enhance by using the non-Fourier's theory.

The heat and mass fluxes model were used by Khan et al. (2017) in constructing the equations of conservation of energy and conservation of mass that contribute to thermal and concentration relaxation time. At the end of their work, HAM was used. Enhancement of parameter of rotation decreases values of axial velocity and the corresponding momentum boundary layer thickness. Similarly, the thermal and concentration relaxation time coefficients decrease the measurement of hotness/coldness and concentration fields. Muhammad et al. (2017) analyzed the nanofluid squeezing flow together with non-Fourier's energy and volume per unit density by developing the modified Fourier's heat flux theory. The features of the velocity are analyzed using heat energy and concentration stratification theory. Effects due to several coefficients against hotness/coldness, particles concentration and velocity profiles are analyzed using graphs. As values of thermal and solutal relaxation parameters increase, then the corresponding hotness/coldness, particles concentration and velocity profiles increase. Both theories of thermal and solutal stratifications are considered in this work.

Von Karman in 1921 introduced the spinning disk flow in fluid mechanics and El-Mistakawy et al. (2000) applied an asymptotic solution for the flow as a result of an infinite rotating disk in the case of small magnetic fields. Hayat et al. (2018a) studied the progress of the quantity of difference (entropy) for Sisko fluid flow. They showed that the velocity and temperature fields are increasing in the case of larger material and temperature ratio parameters. The results obtained are useful in understanding the entropy generation for flows of non-Newtonian fluids. Qayyum et al. (2018) investigated similar thermodynamic entropy in a Williamson flow due to co-spinning disks. They used Karman (1921) transformations and converted the partial differential equations (PDEs) to coupled ODEs which are solved by applying convergent series solutions. They investigated the influence of many concerned parameters against the velocity, degree of entropy of flow hotness/coldness, heat transfer rate and coefficient of skin friction. The conclusion is that tangential velocity and

axial velocity are enhanced when values of Weissenberg number increase and with decreasing axial velocity. The entropy parameter gets larger in Brinkman number, Hartmann number and radiation parameter. Das (2015) undertook a step-by-step analytical solution of the flow in double co-spinning disks, applying HAM. Three different situations were recommended for small Reynolds numbers. Mahmood et al. (2018) analyzed heat transfer with entropy in the boundary layer flow and heat flux theory of Cattaneo-Christov using Casson fluid. They concluded for the velocity to enhance when an injection parameter increases while magnetic effect reduces as the nanofluid flow velocity at the boundary layer region increases.

Dogonchi and Ganji (2017) applied the modified heat flux theory towards magnetohydrodynamic nanofluid flow velocity and heat transfer near dual plates by using radiated heat energy effect with the conclusion that when the Nusselt number increases then the heat source parameter also increases. Upadhyay et al. (2018) investigated the effect of a nonlinear non-steady convection against nanofluids and microfluids using the heat flux theory of Cattaneo-Christov. The conclusion is that less time is taken using nanofluids than microfluids. Mahanthesh et al. (2017) analyzed an upper convected Maxwell fluid flow using two stratifications with a distance dependent heat source and concluded that the axial velocity and tangential velocity enhance as the temperature field decreases when Weissenberg number enhances the value of the Deborah number.

Hayat and Nadeem (2018) studied Eyring-Powell fluid flow in three dimensions by applying the theory of heat flux of Cattaneo-Christov alongside the reactions across a surface stretching with conclusion that the heat is generated more in Fourier's first model as compared to that by Cattaneo and Christov on heat flux. Hayat et al. (2017a) analyzed a 3D Jeffrey nanofluid flow using the heat flux model by Cattaneo-Christov with a result that by using the non-Fourier's heat flux, the axial velocity together with the tangential velocity are enhanced but temperature profile decreases when Weissenberg number enhances the value of Deborah number. Thermal stratification in a stretching flow is analyzed by Hayat et al. (2017b) using the heat flux of Cattaneo-Christov model and it results in temperature decrease as the thermal stratification parameter diminishes. Moving on, Hayat et al. (2018b) were investigating a Jeffrey nanofluid by adding together thermal changing values of diffusion coefficient with Cattaneo-Christov, hence the axial velocity and tangential velocity appeared as decreasing functions of the ratio of relaxation time over retardation time.

Mustafa (2017) used Buongiorno's mathematical model to analyze a magnetohydrodynamic (MHD) nanofluid flow across a spinning disk which is controlled by partial slip effects and concluded that axial velocity and tangential velocity diminish when magnetic field strength and slip velocity parameter also diminish. Presently, we extended the model from Hayat et al. (2017c) by adding a magnetic field into the momentum equation, Cattaneo-Christov heat flux, heat generation and thermal radiation to the energy equation and also by introducing the concentration equation. As a result of this, we are able to introduce new physical parameters as comparison to the earlier study. The new involved physical parameters are Hartmann number, thermal radiation, Eckert number, parameter of heat generation and Lewis number. These parameters are used to investigate their impacts against velocity, temperature, and nanoparticle volume fraction profiles. With the newly added concentration equation, we are able to study the rate of mass transfer which was not studied in the previous literature mentioned above.

An electrically conducting nanofluid flow between two spinning disks embedded in a porous medium at $z = 0$ and $z = h$, respectively, are considered in Figure 1. We shall denote the vertical axis, z being the co-axis between the two disks. The lower disk with an angular velocity denoted by Ω_1 and an upper disk with angular velocity Ω_2 are linearly and radially stretched at the constant velocity rates of a_1 and a_2. The vertical magnetic force applied onto the stretching and spinning disks creates magnetic fields in both radial and angular directions of the flow. We use the cylindrical coordinate system (r, Θ, z) with velocity (u, v, w), respectively. Using the base model by Hayat et al. (2017c) with the present inclusion of mass conservation equation and modified conservation of momentum and heat equations, the following can be written accordingly:

$$\frac{\partial u}{\partial r} + \frac{u}{r} + \frac{\partial w}{\partial z} = 0, \qquad (1)$$

$$u\frac{\partial u}{\partial r} - \frac{v^2}{r} + w\frac{\partial u}{\partial z} = \frac{-1}{\rho}\frac{\partial p}{\partial r} + \nu\left[\frac{\partial^2 u}{\partial r^2} + \frac{1}{r}\frac{\partial u}{\partial r} + \frac{\partial^2 u}{\partial z^2} - \frac{u}{r^2}\right]$$
$$-\left(\frac{\mu}{k_0\rho} + \frac{\sigma B_0^2}{\rho}\right)u, \qquad (2)$$

$$u\frac{\partial v}{\partial r} + \frac{uv}{r} + w\frac{\partial v}{\partial z} = \nu\left[\frac{\partial^2 v}{\partial r^2} + \frac{1}{r}\frac{\partial v}{\partial r} + \frac{\partial^2 v}{\partial z^2} - \frac{v}{r^2}\right] \qquad (3)$$
$$-\left(\frac{\mu}{k_0\rho} + \frac{\sigma B_0^2}{\rho}\right)v$$

$$u\frac{\partial w}{\partial r} + w\frac{\partial w}{\partial z} = -\frac{1}{\rho}\frac{\partial p}{\partial z} + \nu\left[\frac{\partial^2 w}{\partial r^2} + \frac{1}{r}\frac{\partial w}{\partial r} + \frac{\partial^2 w}{\partial z^2}\right] - \frac{\mu w}{k_0\rho} \ , (4)$$

$$u\frac{\partial T}{\partial r} + w\frac{\partial T}{\partial z} = \frac{k}{\rho C_p}\left[\frac{\partial^2 T}{\partial r^2} + \frac{1}{r}\frac{\partial T}{\partial r} + \frac{\partial^2 T}{\partial z^2}\right] + \frac{\sigma B_0^2(u^2+v^2)}{\rho c_p} -$$

$$\gamma\left[u^2\frac{\partial^2 T}{\partial r^2} + w^2\frac{\partial^2 T}{\partial z^2} + 2uw\frac{\partial^2 T}{\partial z\partial r} +\right.$$

$$\left(u\frac{\partial u}{\partial r} + w\frac{\partial u}{\partial z}\right)\frac{\partial T}{\partial r} + \left(u\frac{\partial w}{\partial r} + w\frac{\partial w}{\partial z}\right)\frac{\partial T}{\partial z}\right] + \frac{(\rho c_p)_s}{(\rho c_p)_f}$$

$$\left[D_B\left(\frac{\partial T}{\partial r}\frac{\partial C}{\partial r} + \frac{\partial T}{\partial z}\frac{\partial C}{\partial z}\right) + \frac{D_T}{T_\infty}\left(\left(\frac{\partial T}{\partial r}\right)^2 + \left(\frac{\partial T}{\partial z}\right)^2\right)\right]$$

(5)

$$+ \frac{Q_0(T_1-T_2)}{\rho c_p} - \frac{\partial q_r}{\partial z}\frac{1}{\rho c_p},$$

$$u\frac{\partial C}{\partial r} + w\frac{\partial C}{\partial z} = D_B\left[\frac{\partial^2 C}{\partial r^2} + \frac{1}{r}\frac{\partial C}{\partial r} + \frac{\partial^2 C}{\partial z^2}\right] +$$

$$\frac{D_T}{T_\infty}\left[\frac{\partial^2 T}{\partial r^2} + \frac{1}{r}\frac{\partial T}{\partial r} + \frac{\partial^2 T}{\partial z^2}\right],$$

(6)

FORMULATION OF THE FLOW MODEL

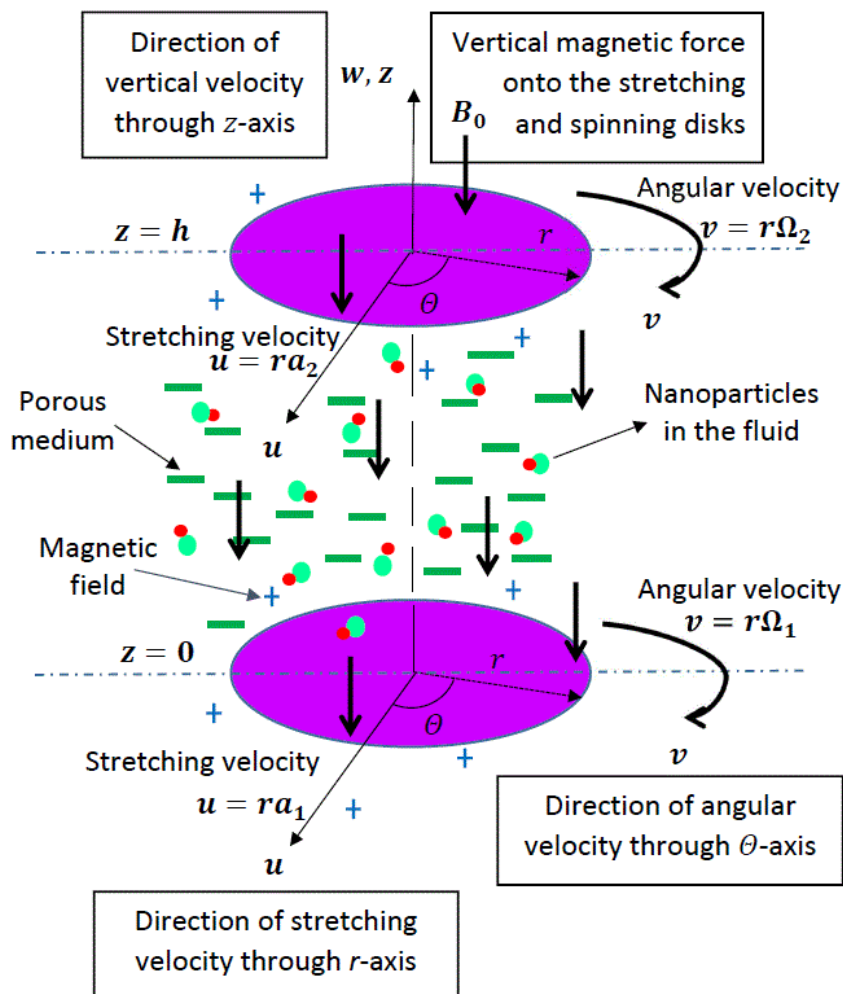

FIGURE 1. The geometry of the model

with boundary conditions:

At $z = 0$; $u = ra_1, v = r\Omega_1, w = 0, T = T_1, C = C_1,$

At $z = h$; $u = ra_2, v = r\Omega_2, w = 0, T = T_2, C = C_2,$ $\qquad$ (7)

where T_1 and T_2 are respective temperatures at the lower and upper disks, C_1 and C_2 are respective concentrations at the lower and upper disks, respectively, C is concentration of the fluid, thermal radiation q_r, pressure p, fluid density ρ, specific heat c_p, kinematic viscosity v, dynamic viscosity μ, permeability constant k_0, fluid thermal conductivity k, electrical conductivity σ, magnetic strength B_0, thermal relaxation time $_\gamma$, nanoparticles heat capacitance $(\rho c_p)_s$, fluid heat capacitance ρc_p, Brownian diffusion coefficient D_B, thermophoresis diffusion coefficient D_T, free stream temperature T_∞ and heat generation coefficient Q_0.

TRANSFORMATION OF SIMILARITY

Using the von Karman transformation (Karman 1921):

$$u = r\Omega_1 f'(\eta), \; v = r\Omega_1 g(\eta), \; w = -2h\Omega_1 f(\eta), \quad (8)$$

$$\theta = \frac{T-T_2}{T_1-T_2}, \phi = \frac{C-C_2}{C_1-C_2}, p = \rho\Omega_1 v[(P(\eta) + \frac{r^2\epsilon}{2h^2}], \eta = \frac{z}{h}.$$

and applying them into (2)-(6), we obtain:

$$f''' + Re(2ff'' - f'^2 + g^2 - \frac{f'}{\beta} - Mf') - \epsilon = 0, \quad (9)$$

$$g'' + Re[2fg' - 2f'g - \frac{g}{\beta} - Mg] = 0, \quad (10)$$

$$P' - Re[2f/\beta - 4ff'] - 2f'' = 0, \quad (11)$$

$$\theta'' + Pr[2Ref\theta' + Nb\theta'\phi' + Nt(\theta')^2] + PrReQ\theta +$$

$$MPrReE_c[(f')^2 + g^2] - 4\lambda PrRe[f^2\theta'' + ff'\theta'] + \quad (12)$$

$$\frac{4\theta''}{3Rd} = 0,$$

$$\phi'' + 2RePrLef\phi' + Nt\theta''/Nb = 0, \quad (13)$$

with boundary conditions,

$$f(0) = 0, f(1) = 0, f'(0) = A_1, f'(1) = A_2,$$

$$g(0) = 1, g(1) = \tau, \theta(0) = 1, \theta(1) = 0, \quad (14)$$

$$P(0) = 0, \phi(0) = 1, \phi(1) = 0,$$

where

$$Pr = \frac{(\rho c_p)v}{k}, Re = \frac{\Omega_1 h^2}{v}, M = \frac{\sigma B_0^2}{\rho\Omega_1}, E_c = \frac{\rho r^2\Omega_1^2}{(\rho c_p)(T_1-T_2)},$$

$$\beta = \frac{k_0\Omega_1}{\mu}, \lambda = \gamma\Omega_1,$$

$$Nb = \frac{(\rho c_p)_s D_B(C_1-C_2)}{v(\rho c_p)}, Nt = \frac{(\rho c_p)_s D_T(T_1-T_2)}{(\rho c_p)v T_\infty}, \quad (15)$$

$$\alpha = \frac{k}{(\rho c_p)}, Le = \frac{\alpha}{D_B},$$

$$Q = \frac{Q_0(T_1-T_2)}{\rho c_p}, A_1 = \frac{a_1}{\Omega_1}, A_2 = \frac{a_2}{\Omega_2}, \tau = \frac{\Omega_2}{\Omega_1}.$$

$f(\eta)$, $g(\eta)$, $\theta(\eta)$ and $\phi(\eta)$ are the dimensionless velocity, tangential velocity, temperature and concentration functions. Moreover, we define Prandtl number Pr, porosity parameter β, Hartmann number M, Reynolds number Re, local Eckert number E_c, Brownian parameter Nb, thermophoresis parameter Nt, thermal diffusivity α, Lewis number Le, thermal relaxation time parameter λ, disk rotation ratio τ, thermal radiation parameter Rd, heat generation/absorption parameter Q, pressure parameter ϵ and the velocity ratios of stretching and angular spinning for the lower and upper disks are A_1 and A_2, respectively. From Hayat et al. (2018c), the rates of heat transfer at the lower and upper disks are given as:

$$Nu_{x1} = \frac{h_1 q_w|_{z=0}}{k(T_1-T_2)}, Nu_{x2} = \frac{h_2 q_w|_{z=h}}{k(T_1-T_2)}, \quad (16)$$

where q_w is the heat flux defined by

$$q_w|_{z=0} = -k\frac{\partial T}{\partial z} = -k\frac{(T_1-T_2)\theta'(0)}{h_1}, \quad (17)$$

$$q_w|_{z=h} = -k\frac{\partial T}{\partial z} = -k\frac{(T_1-T_2)\theta'(1)}{h_2}.$$

Using equations (17) in (16) we get,

$$Nu_{x1} = -\theta'(0), Nu_{x2} = -\theta'(1), \quad (18)$$

which is non-dimensional form of Nusselt numbers at the lower and upper disks, respectively. We may rewrite equation (9) in such a way that if we remove ϵ and by differentiating it subject to η, we may obtain,

$$f^{iv} + Re[2ff''' + 2gg' - \frac{f''}{\beta} - Mf''] = 0. \quad (19)$$

The stresses of shear at the lower disk are in the radial and azimuthal directions, as as τ_{zr} and $\tau_{z\theta}$, respectively, and are perpendicular to one another and therefore

$$\tau_{zr} = \nu \frac{\partial u}{\partial z}|_{z=0} = \nu \frac{r\Omega_1 f''(0)}{h}, \tau_{z\theta} = \nu \frac{\partial v}{\partial z}|_{z=0} = \nu \frac{y\Omega_1 g'(0)}{h}. \quad (20)$$

Therefore, the total stress acting on the lower disk is,

$$\tau_w = \sqrt{\tau_{zr}^2 + \tau_{z\theta}^2}. \quad (21)$$

At the lower and upper disks, the skin frictions are:

$$C_{f1} = \frac{\tau_w|_{z=0}}{\rho(r\Omega_1)^2} = \frac{\sqrt{[(f''(0))^2 + (g'(0))^2]}}{R_{er}},$$
$$C_{f2} = \frac{\tau_w|_{z=h}}{\rho(r\Omega_2)^2} = \frac{\sqrt{(f''(1))^2 + (g'(1))^2}}{R_{er}}, \quad (22)$$

where R_{er} is the local Reynolds number, $Re_r = \frac{\Omega_1 h r}{\mu}$. The Sherwood number is defined as:

$$Sh = \frac{q_m h}{D_B(C_1 - C_2)}, q_m = -\frac{D_B}{h}\frac{\partial C}{\partial z}. \quad (23)$$

This gives $Sh = -\phi(\eta)$, hence at the lower and upper disks, $Sh_1 = -\phi'(0)$ and $Sh = -\phi'(1)$.

COMPUTATIONAL METHOD

A finite-difference based MATLAB function $bvp4c$ method with shooting technique is applied to equations (9) to (14) and (19) with results:

$$f = f_1, f' = f_2, f'' = f_3, f''' = f_4, f^{iv} = AA_1, \quad (24)$$

$$g = f_5, g' = f_6, g'' = AA_2, \quad (25)$$

$$P = f_7, P' = AA_3 \quad (26)$$

$$\theta = f_8, \theta' = f_9, \theta'' = AA_4, \quad (27)$$

$$\phi = f_{10}, \phi' = f_{11}, \phi'' = AA_5. \quad (28)$$

Substituting (24) to (28) into (9) to (14), we now obtain:

$$AA_1 = Re\left(\frac{f_3}{\beta} + Mf_3 - f_1 f_4 - 2f_5 f_6\right), \quad (29)$$

$$AA_2 = Re\left(2f_2 f_5 + \frac{f_5}{\beta} + Mf_5 - 2f_1 f_6\right), \quad (30)$$

$$AA_3 = Re\left(\frac{2f_1}{\beta} - 4f_1 f_2\right) + 2f_3, \quad (31)$$

$$AA_4 = 3Pr$$

$$\left(\frac{4\lambda Re f_1 f_2 f_9 - MRe E_c(f_2^2 + f_5^2) - (2Re f_1 f_9 + Nb f_9 f_{11} + Nt f_9^2) - Re f_8 Q}{(3 + 4Rd - 12\lambda Pr Re f_1^2)}\right), \quad (32)$$

$$AA_5 = -3NtPr$$

$$\left(\frac{4\lambda Re f_1 f_2 f_9 - MRe E_c(f_2^2 + f_5^2) - (2Re f_1 f_9 + Nb f_9 f_{11} + Nt f_9^2) - Re f_8 Q}{Nb(3 + 4Rd - 12\lambda Pr Re f_1^2)}\right) (33)$$

RESULTS AND DISCUSSION

In this section, we present tables and figures to analyse the behaviour of velocity, temperature, concentration profiles and skin friction, for different involved parameters. Unless stated otherwise, we used the following fixed parameters' values for all the tables and figures presented: $Nb = 0.5$, $Re = Nt = 0.4$, $M = Pr = A_1 = 0.3$, $A_2 = 0.2$, $\beta = 0.1$, $Q = 0.03$, $Rd = 0.02$, $\lambda = Le = E_c = \tau = 0.01$. Comparisons of the present skin friction values along the radial and tangential velocities with the results by Stewartson (1953) and homotopy solutions by Imtiaz et al. (2016) at $z = 0$ when $A_1 = A_2 = \phi = 0$ and $Re = 1$ are presented in Table 1. Good agreements in the results are perceived.

TABLE 1. Comparing skin friction along the radial and tangential velocities

τ	$f''(0)$	$-g'(0)$	$f''(0)$	$-g'(0)$	$f''(0)$	$-g'(0)$
	Stewartson (1953)		Imtiaz et al. (2016)		Present	
-1	0.06666	2.00095	0.6666	2.00095	0.06666	2.00095
-0.8	0.08394	1.80259	0.08394	1.80259	0.08394	1.80259
-0.3	0.10395	1.30442	0.10395	1.30442	0.10395	1.30443
0	0.09997	1.00428	0.09997	1.00428	0.09997	1.00428
0.5	0.06663	0.50261	0.06663	0.50261	0.06663	0.50262

TABLE 2. Comparing physical quantities with changing values of Re

Re	τ	$f''(0)$	$g'(0)$	$-\theta'(0)$	$f''(0)$	$g'(0)$	$-\theta'(0)$	$f''(0)$	$g'(0)$	$-\theta'(0)$
		Turkyilmazoglu (2016)			Ahmed et al. (2019)			Present		
0	-0.5	-2.000007	1.50000	1.050810	-2.00000	1.500000	1.0000	-2.0000	1.50000	1.00000
10		-1.605628	3.40116	1.050012	-1.605632	3.401195	1.05001	-1.60563	3.40116	1.00000
0	0.0	-2.000007	1.00000	1.050810	-2.00000	1.00000	1.00000	-2.00000	1.00000	1.00000
10		-1.4456172	2.56217	1.055826	-1.445607	2.562188	1.05582	-1.44562	2.56217	1.00000
0	0.5	-2.000007	0.50000	1.050810	-2.0000	0.5000	1.00000	-2.0000	0.50000	1.00000
10		-1.8945983	1.50020	1.052580	-1.89458	1.500226	1.05258	-1.8946	1.5002	1.00000

TABLE 3. Impact of different physical parameters against rates of heat transfer at the lower and upper spinning disks

M	E_c	Rd	Q	A_2	β	Nu_{x1}	Nu_{x2}
2.1	0.8	0.6	0.3	0.5	0.8	0.45565	0.46321
1.5						0.45780	0.46535
1.3						0.45852	0.46607
2.1	0.9					0.45472	0.46227
	1.0					0.45378	0.46135
	0.8	0.7				0.47953	0.8765
		0.8				0.47953	0.51019
		1.1				0.50153	0.51019
		0.6	0.4			0.55810	0.56314
			0.6			0.45536	0.46291
			0.7	0.9		0.45476	0.46231
				1.0		0.45506	0.46261
				0.5	0.9	0.45487	0.46242
					1.0	0.45497	0.46251
					0.8	0.45423	0.46178

Extended comparisons are done in Table 2 with exact solutions by Turkyilmazoglu (2016) and MATLAB *bvp4c* solutions by Ahmed et al. (2019) for diverse values of Re when $A_1 = 0.5$ and $A_2 = 0.0$. Good agreements are perceived from these tables and thus present computations have been validated. Table 3 depicts the impact of different physical parameters against rates of heat transfer at the lower and upper spinning disks. These rates increase with increasing M but decrease when the corresponding values of porosity parameter increase. Table 4 validates present works with Hayat et al. (2017c) who used Homotopy Analysis Method (HAM) and Table 5 shows impacts of different physical parameters against rates of mass transfer at the lower and upper spinning disks. These rates increase with an increase in local Eckert number E_c but decrease with an increase in heat generation parameter Q.

TABLE 4. Comparing skin friction values at the lower and upper spinning disks

β	A_2	Re	A_1	τ	C_{f1}	C_{f2}	C_{f1}	Cf_2
					Hayat et al. (2017)		Present	
0.90	0.4	0.01	0.4	0.8	2.408261	2.409302	2.4107	2.4026
1.0					2.408173	2.40897	2.4106	2.4025
1.1					2.40810	2.409293	2.4105	2.4024
0.9	0.5				2.607280	2.808393	2.60800	2.6007
	0.6				2.806356	3.207768	2.80890	2.7988
	0.4	0.1			2.408024	2.418446	2.43520	2.4269
		0.2			2.409185	2.429209	2.4690	2.46470
		0.01	0.5		2.807095	2.608926	2.80990	2.8008
			0.6		3.206236	2.808676	3.20940	3.1993
			0.4	0.9	2.4018558	2.403112	2.40400	2.4014
				1.0	2.399810	2.401089	2.4014	2.3933

TABLE 5. Impact of different physical parameters against rates of mass transfer at the lower and upper spinning disks

M	E_c	Rd	Nb	Q	Nt	$-\phi'(0)$	$-\phi'(1)$
0.8	0.5	0.4	0.2	0.4	0.3	2.598510	2.564848
0.9						2.636753	2.602218
1.1						2.710084	2.673782
0.8	0.8					2.808543	2.789740
	1.2					3.088276	3.066776
	1.5					3.297841	3.274324
	0.5	0.6				2.366013	2.336249
		0.7				2.273359	2.245253
		0.8				2.206500	2.179244
		0.4	0.6			1.628526	1.617694
			0.8			1.500320	1.492481
			0.2	0.5		2.596079	2.563159
				0.6		2.594134	2.561940
				0.7		2.592725	2.577017
				0.8	0.5	3.889817	3.834104

Figure 2(a) shows the impact of Hartmann number M on axial velocity. The axial velocity increases with an increase in values of M. Figure 2(b) depicts the influence of A_2 against the radial velocity. As the velocity ratio A_2 increases, the corresponding radial velocity enhances at the upper disk. The velocity ratio exhibits a dual impact on A_2. This is obvious as the ratio oscillates from the negative sign at the lower disk to the positive sign in the neighbourhood of the upper disk. This is the result of increasing values of A_2. The physical meaning is that the fluid bounded by both disks continues to bounce in opposite directions, from the lower disk to the upper disk, in the midway of the fluid neighbourhood. Figure 2(c) depicts the influence of Nt on particle concentration and Figure 2(d) shows thermal relaxation time parameter λ impacting on temperature profile. Both parameters caused reduction in those concentration and temperature profiles as they increase. This is due to the fact that thermophoresis promotes migration of nanoparticles thus the flow concentration is banished as time increases. With prolonged thermal relaxation, more heat can be transferred to surrounding and as a result, temperature decays.
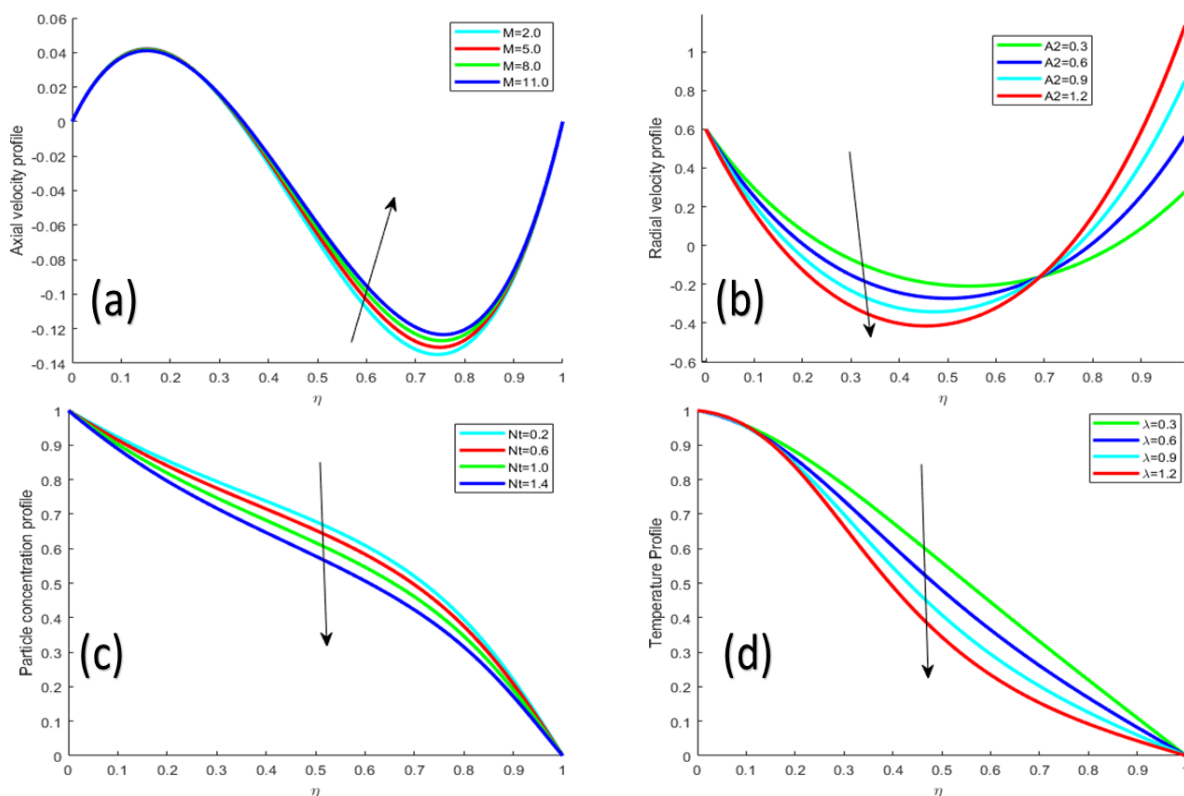

FIGURE 2. Impacts of (a) Hartmann number on axial velocity, (b) upper disk velocity ratio on radial velocity, (c) thermophoresis diffusion parameter on concentration and (d) thermal relaxation on temperature

Figure 3(a) shows the impact of heat generation parameter Q on temperature profile. When value of Q increases then the corresponding temperature profile also increases. The boundary layer thickness and heat energy increase whenever the value of Q increases. Thus, the nanofluid flow becomes hotter. Figure 3(b) shows the impact of Q on the nanoparticle concentration where it decreases as Q increases in value and the nanoparticles concentration is distributed throughout the fluid body. Figure 3(c) exhibits the impact of E_c on temperature profile. When E_c increases, then the internal energy of the system increases as additional nanoparticles to the base fluid will cause the bonds of the base fluid to break creating more energy, hence the temperature profile increases. Mechanically, the action of the internal friction of molecules causes the mechanical fluid energy to transform into thermal energy. Figure 3(d) shows the impact of E_c on nanoparticle concentration. Owing to similar justification to the heat generation, as the value of local Eckert number E_c increases, the corresponding nanoparticle concentration profile also decreases in value.
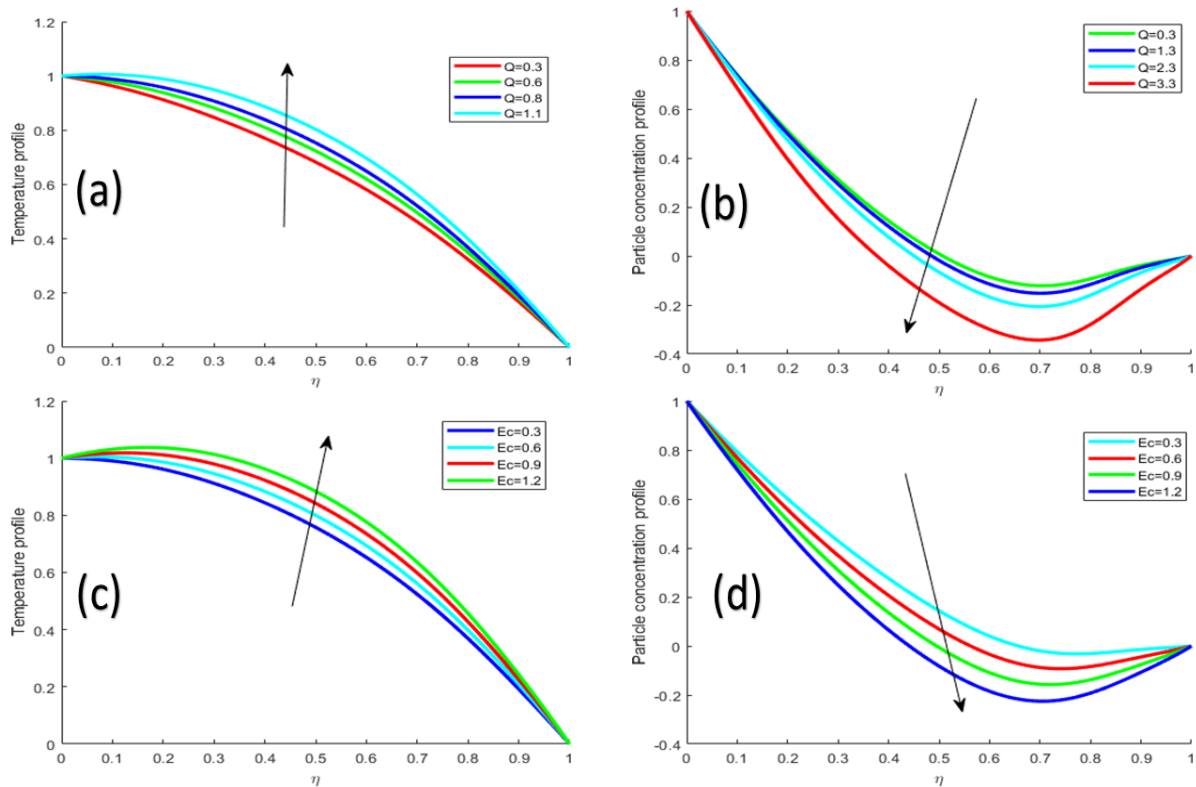
FIGURE 3. Impacts of (a) heat generation parameter on temperature and (b) concentration, (c) local Eckert number on temperature and (d) concentration

Figure 4(a) shows the impact of thermal radiation Rd on temperature, whereby the temperature profile is displayed as a decreasing function of Rd. It occurs as a result of heat being disposed off to surroundings much faster with help of higher radiation mechanism. Thermal radiation impacting concentration is depicted in Figure 4(b). This shows the concentration profile as an increasing function of Rd. Since the flow becomes cooler, it attracts nanoparticles' settlement at the lower spinning disk thus concentration increases. Figure 4(c) demonstrates the impact of Pr on the fluid flow hotness or coldness profile. Increasing Princreases the temperature profile because it indicates thermal heat will be diffused to surroundings slowly as the momentum diffusivity increases. Figure 4(d) shows the concentration profile decreases as Pr increases. This is due to the fact that hotter fluid incites the high kinetic nanoparticles to scatter throughout the fluid flow and weaken the accumulation of nanoparticles at a point in between the two spinning disks.

Based on Figure 5(a)-5(c), the growing values of all three parameters of Brownian diffusion Nb, thermophoresis diffusion Nt and rotation ratio τ have significant contributions towards increasing the fluid hotness. An increase in Brownian diffusion coefficient produces more momentum clashes and irregular motions of the nanoparticles which create an internal source energy to steam the fluid thermodynamics. Temperature profile is an increasing function of thermophoresis parameter. The physical reason is that it requires additional thermal energy to enable mass transport of the nanoparticles from the hotter environment to the cooler one. As values of rotation number increase, the corresponding values of temperature profile also increase because more rotation movements are created thus the crave for additional thermal energy is mounting and therefore, the temperature profile increases. Finally, Figure 5(d) shows the impact of Hartmann number M on the tangential velocity. Undoubtedly, the velocity decreases when M increases because more frictions are devised which oppose the movement of the flow, and so the nanofluid moves slowly.
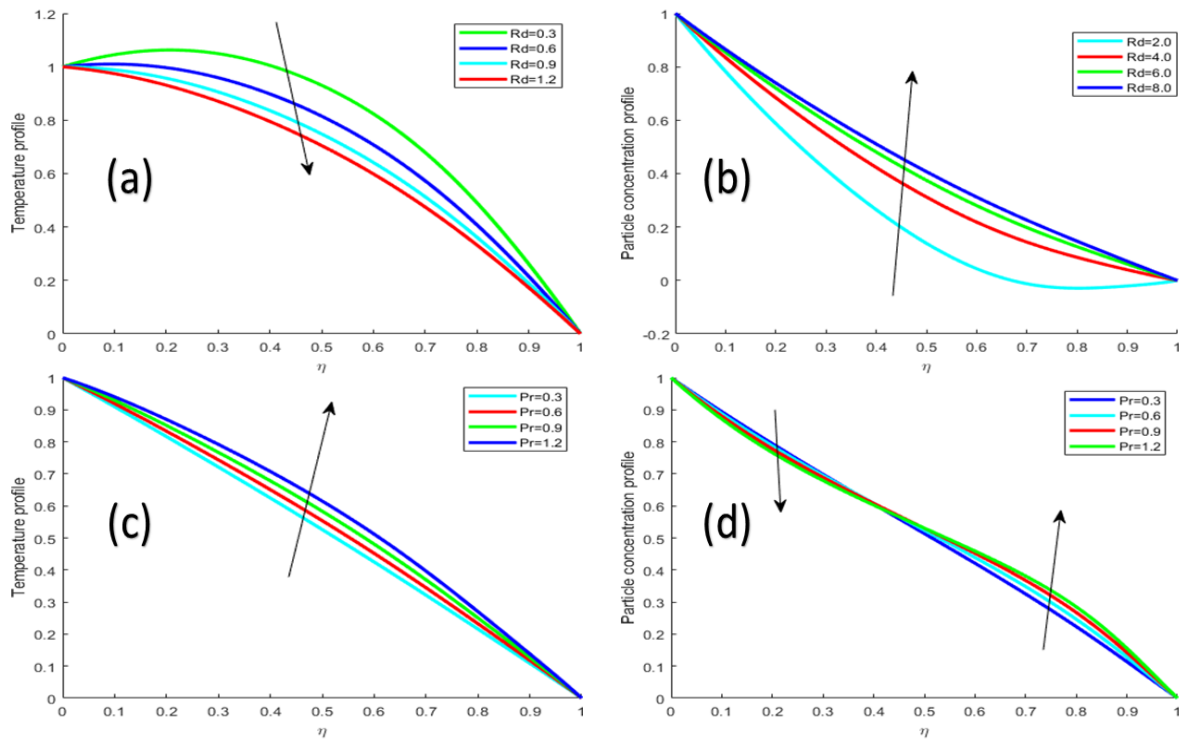
FIGURE 4. Impacts of (a) thermal radiation on temperature and (b)
concentration, (c) Prandtl number on temperature and (d) concentration
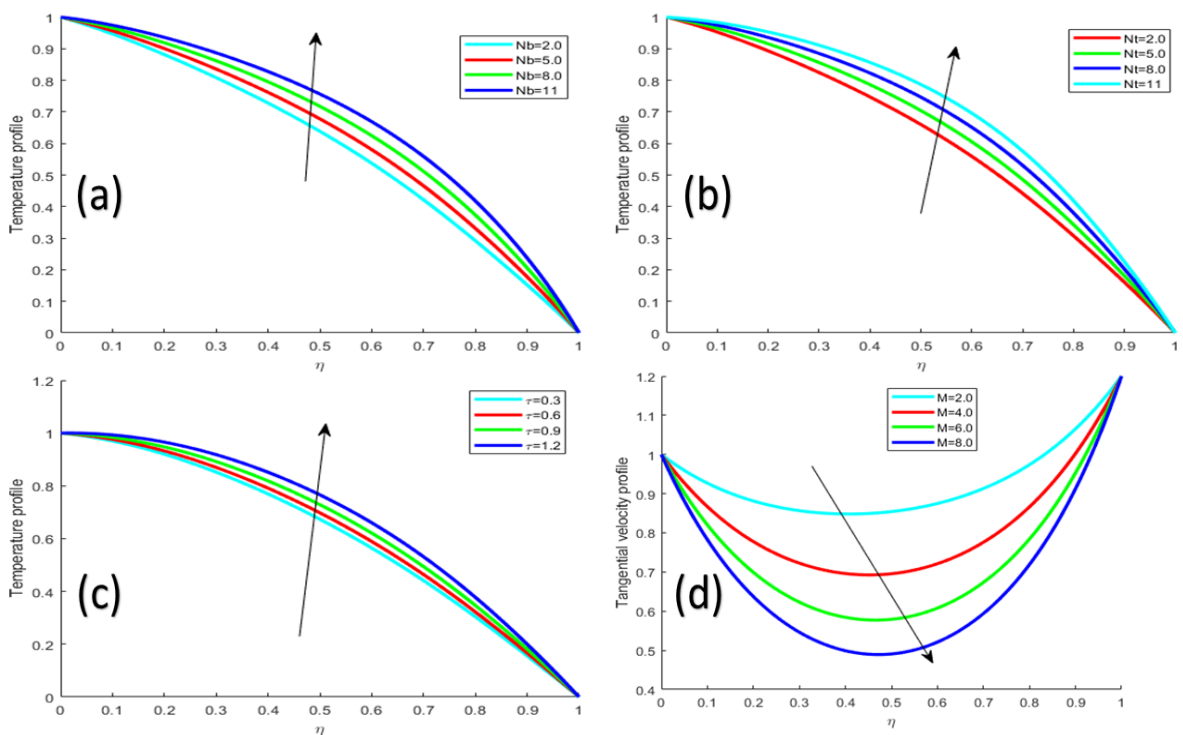

FIGURE 5. Impacts of (a) Brownian diffusion, (b) thermophoresis
diffusion and (c) disk rotation ratio on temperature and (d) Hartmann
number on tangential velocity

CONCLUSION

We have studied thermal radiation, heat generation with an applied field of magnets together with the transport equation and Cattaneo-Christov heat flux of a Buongiorno's nanofluid flow embedded in a Darcian porous medium between two stretchable spinning disks, with conclusions as follows. Increasing Hartmann number or magnetic field will increase the axial velocity but to decrease the tangential velocity of the nanofluid flow due to the applied field of magnets produces resistances to oppose the fluid dynamics. An increase in the stretching parameter oscillates the radial velocity from negative to positive values. The nanofluid is cooling with prolonged thermal radiation and thermal relaxation from Cattaneo-Christove heat flux, but boiling with growing heat generation, Eckert number, Prandtl number, Brownian diffusion, thermophoresis diffusion and rotation ratio. The concentration profiles can be trimmed down with higher thermophoresis diffusion, heat generation, heat transfer dissipation (due to local Eckert number) and momentum diffusivity (due to Prandtl number). Oppositely, this concentration distribution can be enhanced with higher thermal radiation. The present study is significant due to its feasible applications in engineering and industries. Some of the applications are in food processing, magnetic storage devices, electronic devices with rotary parts, and gas turbine engines. The findings are relevant with the development of concentration and thermal systems.

REFERENCES

Ahmed, J., Khan, M. & Ahmad, L. 2019. MHD swirling flow and heat transfer in Maxwell fluid driven by two coaxially rotating disks with variable thermal conductivity. *Chin. J. Phys.* 60: 22-34.

Das, A. 2015. Analytical solution to the flow between two coaxial rotating disks using HAM. *Procedia Eng.* 127: 377-382.

Dogonchi, A. & Ganji, D. 2017. Impact of Cattaneo-Christov heat flux on MHD nanofluid flow and heat transfer between parallel plates considering thermal radiation effect. *J. Taiwan Inst. Chem. Eng.* 80: 52-63.

El-Mistakawy, T.M., Attia, H.A. & Megahed, A.A. 2000. Asymptotic solution for the flow due to an infinite rotating disk in the case of large magnetic field. *Trans. Can. Soc. Mech. Eng.* 24: 515-523.

Hayat, T. & Nadeem, S. 2018. Flow of 3D Eyring-Powell fluid by utilizing Cattaneo-Christov heat flux model and chemical processes over an exponentially stretching surface. *Results Phys.* 8: 397-403.

Hayat, T., Khan, M.I., Qayyum, S., Khan, M.I. & Alsaedi, A. 2018a. Entropy generation for flow of Sisko fluid due to rotating disk. *J. Mol. Liq.* 264: 375-385.

Hayat, T., Javed, M., Imtiaz, M. & Alsaedi, A. 2018b. Effect of Cattaneo-Christov heat flux on Jeffrey fluid flow with variable thermal conductivity. *Results Phys.* 8: 341-351.

Hayat, T., Khan, M.W.A., Khan, M.I., Waqas, M. & Alsaedi, A. 2018c. Impact of chemical reaction in fully developed radiated mixed convective flow between two rotating disk. *Physica B Condens.* 538: 138-149.

Hayat, T., Muhammad, T., Mustafa, M. & Alsaedi, A. 2017a. Three-dimensional flow of Jeffrey fluid with Cattaneo-Christov heat flux: An application to non-Fourier heat flux theory. *Chin. J. Phys.* 55(3): 1067-1077.

Hayat, T., Khan, M.I., Farooq, M., Alsaedi, A. & Khan, M.I. 2017b. Thermally stratified stretching flow with Cattaneo-Christov heat flux. *Int. J. Heat Mass Transfer* 106: 289-294.

Hayat, T., Qayyum, S., Imtiaz, M. & Alsaedi, A. 2017c. Flow between two stretchable rotating disks with Cattaneo-Christov heat flux model. *Results Phys.* 7: 126-133.

Imtiaz, M., Hayat, T., Alsaedi, A. & Ahmad, B. 2016. Convective flow of carbon nanotubes between rotating stretchable disks with thermal radiation effects. *Int. J. Heat Mass Transfer* 101: 948-957.

Jyothi, K., Reddy, P.S. & Reddy, M.S. 2018. Influence of magnetic field and thermal radiation on convective flow of SWCNTs-water and MWCNTs-water nanofluid between rotating stretchable disks with convective boundary conditions. *Powder Tech.* 331: 326-337.

Karman, T.V. 1921. Über laminare und turbulente Reibung. *ZAMM* 1(4): 233-252.

Khan, W., Irfan, M. & Khan, M. 2017. An improved heat conduction and mass diffusion models for rotating flow of an Oldroyd-B fluid. *Results Phys.* 7: 3583-3589.

Khan, W.A., Khan, M. & Alshomrani, A.S. 2016. Impact of chemical processes on 3D Burgers fluid utilizing Cattaneo-Christov double-diffusion: Applications of non-Fourier's heat and non-Fick's mass flux model. *J. Mol. Liq.* 223: 1039-1047.

Mahanthesh, B., Gireesha, B. & Raju, C. 2017. Cattaneo-Christov heat flux on UCM nanofluid flow across a melting surface with double stratification and exponential space dependent internal heat source. *Inform. Med. Unlocked* 9: 26-34.

Mahmood, A., Jamshed, W. & Aziz, A. 2018. Entropy and heat transfer analysis using Cattaneo-Christov heat flux model for a boundary layer flow of Casson nanofluid. *Results Phys.* 10: 640-649.

Muhammad, N., Nadeem, S. & Mustafa, T. 2017. Squeezed flow of a nanofluid with Cattaneo-Christov heat and mass fluxes. *Results Phys.* 7: 862-869.

Mustafa, M. 2017. MHD nanofluid flow over a rotating disk with partial slip effects: Buongiorno model. *Int. J. Heat Mass Transfer* 108: 1910-1916.

Qayyum, S., Khan, M.I., Hayat, T., Alsaedi, A., Tamoor, M. 2018. Entropy generation in dissipative flow of Williamson fluid between two rotating disks. *Int. J. Heat Mass Transfer* 127: 933-942.

Stewartson, K. 1953. On the flow between two rotating coaxial disks. *Mathematical Proceedings of the Cambridge Philosophical Society*. Cambridge University Press: Cambridge, UK. pp. 333-341.

Turkyilmazoglu, M. 2016. Flow and heat simultaneously induced by two stretchable rotating disks. *Phys. Fluids* 28(4): 043601.

Upadhya, S.M., Raju, C. & Saleem, S. 2018. Nonlinear unsteady convection on micro and nanofluids with Cattaneo-Christov heat flux. *Results Phys.* 9: 779-786.

*Corresponding author; email: drfadiya@um.edu.my